

On effects of rail fastener failure on vehicle/track interactions

Lei Xu*, Jianmin Gao and Wanming Zhai

Train and Track Research Institute, State Key Laboratory of Traction Power, Southwest Jiaotong University,
No. 111, North Section 1, Erhuan Road, Chengdu 610031, China

(Received March 4, 2017, Revised May 28, 2017, Accepted May 30, 2017)

Abstract. Rail support failure is inevitably subjected to track geometric deformations. Due to the randomness and evolutions of track irregularities, it is naturally a hard work to grasp the trajectories of dynamic responses of railway systems. This work studies the influence of rail fastener failure on dynamic behaviours of wheel/rail interactions and the railway tracks by jointly considering the effects of track random irregularities. The failure of rail fastener is simulated by setting the stiffness and damping of rail fasteners to be zeroes in the compiled vehicle-track coupled model. While track random irregularities will be transformed from the PSD functions using a developed probabilistic method. The novelty of this work lays on providing a method to completely reveal the possible responses of railway systems under jointly excitation of track random irregularities and rail support failure. The numerical results show that rail fastener failure has a great influence on both the wheel/rail interactions and the track vibrations if the number of rail fastener failure is over three. Besides, the full views of time-dependent amplitudes and probabilities of dynamic indices can be clearly presented against different failing status.

Keywords: vehicle/track interaction; rail fastener failure; track random irregularity; probabilistic method; power spectral density

1. Introduction

With the development of high-speed lines accompanied by larger corridor passengers and axle loads, there is increasing demand on serviceability of railroad infrastructures and its components. To ensure the safety of transportation of passengers and freights, investigations have been carried out on the prediction of dynamic behaviours of the railway vehicles and the tracks when facing with unavoidable failure of track substructures, except for the attention on the parametric design and maintenance of railways (Li *et al.* 2016, Hussein *et al.* 2016).

As one of the most important components of track infrastructures, rail fastener, as shown in Fig. 1, effectively provides a bond between the rails and the under-rail foundations, guarantees the proper track geometries and offers reliably structural flexibility. Thus, there are great concerns on the dynamic characteristic of rail fastener and its influence on vehicle-track dynamic behaviours at present. To date, some researchers have been conducted in this field, see, for instance, Domingo *et al.* (2014) studied the changes in the modal parameters of the rails caused by the transverse cracks of the rails. Chen *et al.* (2014) presented parametric studies on concrete crossties and fastening systems by developing the detailed finite element (FE) model to improve the knowledge regarding the mechanical behaviours of systems. Carrascal *et al.* (2016) focused the work on the influence of the presence of sand

on the dynamic behavior of the fastening system. Thompson *et al.* (1997) considered the important role of elasto-metric pads in determining the dynamic behavior of railway track, and investigated the behaviour of rail fasteners at high frequencies for noise prediction. Zhu *et al.* (2015) established a nonlinear and fractional derivative viscoelastic (FDV) model to analyse the complex behaviour of rail pads with being implemented into the coupled vehicle-track systems. Björn *et al.* (2015) investigated the influence of rail fastener stiffness on track stiffness and contact forces through a validated railway vehicle-turnout interaction model. Xiao *et al.* (2007) developed a nonsymmetrical coupled vehicle/track model to analyse the effect of disabled fastening systems and ballast on railway vehicle derailment. Ilias (1999) used a time domain model accounting for the contact non-linearities to investigate the influence of the railpad stiffness on vehicle/track interaction and corrugation growth. Oregui *et al.* (2015) investigated the influence of modeling the fastening with solid railpads on the vertical dynamics of railway tracks with monoblock sleepers. Some other literatures focused on the measurements of dynamic properties of rail fastener systems, see Smutny (2004), Maes *et al.* (2006).

The researches above illustrate the sensitivity of variation of rail fastener system on performance of railway vehicles and the tracks, and have presented advanced models to survey the dynamic interactions between the railway vehicles and tracks when rail fastener system is involved in the dynamics. But, another very important factor that affects railway vehicle-track interactions, i.e., track random irregularities, hasn't been fully exposed in the analysis (Zhu *et al.* 2015). Xiao *et al.* (2007) directly ignored the influence of track irregularities by applying an

*Corresponding author, Ph.D. Student
E-mail: leix_2014@my.swjtu.edu.cn



Fig. 1 Rail fastener system of slab track system

initial lateral load to excite the wheel-sets. However, track random irregularities are objectively formed and will be continuously growing on rail surfaces. All time-domain dynamic behaviours of railway vehicle/track interaction in simulation or measurement should properly consider the functionality of rail profile deformations. With the participation of track irregularities or not, the dynamic performance of railway systems may be completely different.

Therefore, this present work will put more perspectives on how to capture the full view of dynamic behaviours of railway vehicle-track systems when jointly accounting for the effects of rail fastener failure and track random irregularities. This paper is organized as:

- 1) Formulate the Eqs. of motion for a coupled vehicle-track system (CVTS) with track irregularities as excitation;
- 2) Develop a probabilistic method to simulate track random irregularities;
- 3) Introduce a simple way to model rail fastener failure;
- 4) Conduct numerical studies and concluding remarks.

2. Vehicle-track coupled model

Conventionally, the parameters of railway vehicles and the tracks are set to be constant and uniformly distributed along the railroad, and the vehicle-track dynamic model can be divided into two-dimensional/three-dimensional (2-D/3-D) model according to the motions of vehicle-track systems, and linear/non-linear model according to the modelling of wheel/rail contacts.

The vehicle sub-system and track sub-system are both constructed by linear models, however, with nonlinearity at the wheel-rail contact interfaces decided by the relations between the contact forces and displacement/creepage) (Andersson *et al.* 2015).

2.1 Vehicle and track models

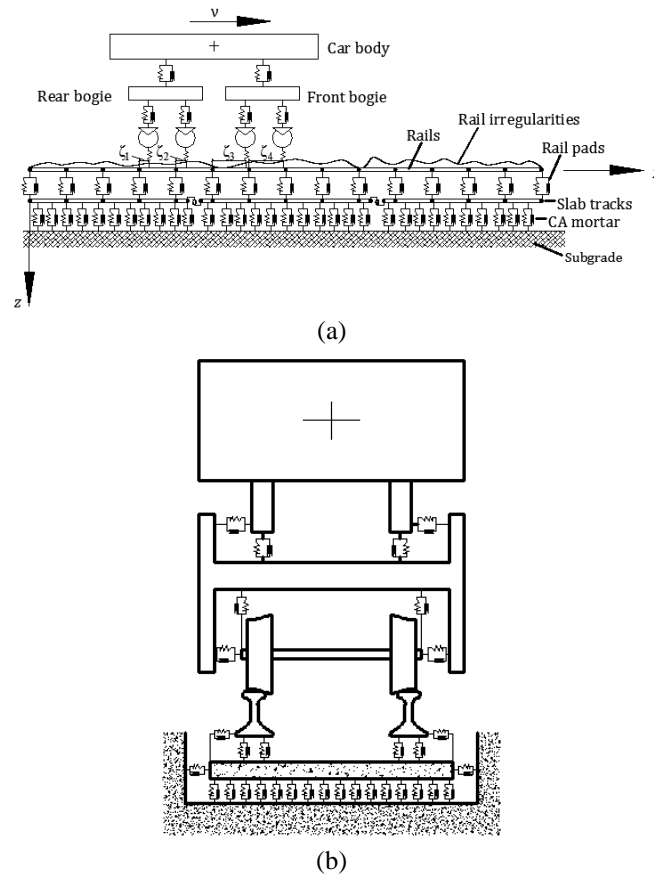


Fig. 2 Three-dimensional vehicle-slab track coupled model: (a): side view; (b) end view

In the present study, it is assumed that a moving vehicle runs with a constant velocity v on typical high-speed slab-track guiding systems, as shown in Fig. 2. In this model, the railway vehicle is constructed as a four-axle mass-spring-damper multi-rigid-body system including a car body, two bogie frames, four wheel sets and two stage suspensions. Each rigid component has 5 degrees of freedom (DOF), namely motions of traverse Y , bounce Z , roll Φ , yaw ψ and pitch β , with respect to their mass centroids. Moreover, the ballastless track system is modelled by finite element method (FEM) (Zeng *et al.* 2015, Xu and Zhai 2016). The track sub-model consists of rails, rail pads, track slabs, CA mortar and subgrade bearing layers, in which the finite elements of beam and thin plate are applied to describe the dynamic characteristics of rails and track slabs, respectively, the subgrade layer is set to be a constraint element. These elements are connected by linear springs and dashpots.

For readers who are interested in the construction of vehicle and track systems, more details can be consulted in the literature (Xu and Zhai 2016).

2.2 Load vectors of wheels and rails

In the vehicle-track coupled model, a precise approach to characterize the wheel-rail spatial and nonlinear interactions is perhaps the most important and complex part. In this work, a new wheel-rail coupling model

developed by Chen and Zhai (2004) is introduced to consider the vertical, lateral and torsional motions of the rail and their interactions to the motions of wheel-sets for spatially coupling the vehicle sub-system and track sub-system at the 3-D wheel-rail interfaces.

The wheel-rail interaction forces mainly include wheel-rail normal contact forces derived by nonlinear Hertzian elastic contact theory according to the elastic compression deformation of wheels and rails at contact points in the normal directions, and tangential wheel-rail creep forces, which are calculated first by the use of Kalker's linear creep theory and then modified by the Shen-Hedrick-Elkins nonlinear model (Shen *et al.* 1983).

Load vector of vehicle and track sub-system represented by \mathbf{F}_V and \mathbf{F}_T can be obtained in (Xu and Zhai 2017).

2.3 The equations of motion of vehicle-track coupled system

Through the work briefly presented in Subsections 2.1 and 2.2, one can derive the equations of motion for vehicle-track interaction system by coupling \mathbf{F}_V , \mathbf{F}_T and matrices of mass, stiffness and damping of vehicle-track systems, which is written in sub-matrix form as (Zhai *et al.* 2009)

$$\begin{bmatrix} \mathbf{M}_V & \mathbf{0} \\ \mathbf{0} & \mathbf{M}_T \end{bmatrix} \begin{Bmatrix} \ddot{\mathbf{X}}_V \\ \ddot{\mathbf{X}}_T \end{Bmatrix} + \begin{bmatrix} \mathbf{C}_V & \mathbf{0} \\ \mathbf{0} & \mathbf{C}_T \end{bmatrix} \begin{Bmatrix} \dot{\mathbf{X}}_V \\ \dot{\mathbf{X}}_T \end{Bmatrix} + \begin{bmatrix} \mathbf{K}_V & \mathbf{0} \\ \mathbf{0} & \mathbf{K}_T \end{bmatrix} \begin{Bmatrix} \mathbf{X}_V \\ \mathbf{X}_T \end{Bmatrix} = \begin{Bmatrix} \mathbf{F}_V \\ \mathbf{F}_T \end{Bmatrix} \quad (6)$$

where the subscripts 'V' and 'T' denote the vehicle sub-system and track sub-system, respectively, \mathbf{M} , \mathbf{C} and \mathbf{K} denote the mass, damping and stiffness sub-matrices respectively, \mathbf{X} and \mathbf{F} denote the displacement and force sub-vectors, respectively.

3. Method for simulating track random irregularities

3.1 Representation of track random irregularities using power spectral densities (PSDs)

Due to the fact that the wheel-rail interactions are significantly affected by both the amplitude and the wavelength of track irregularities, and power spectral density (PSD) of track irregularity is popularly used as the amplitude-frequency representations of track irregularities. In Zhai *et al.* (2009), track irregularity PSD in frequency domain are equivalently transformed into time-domain track irregularities for step-by-step integrations.

Generally, the track irregularity vector used as the loads of vehicle-track coupled system can be expressed by (Xu and Zhai 2017)

$$\left\{ \begin{aligned} \Theta(n, s) &= (\kappa_1(n, s), \kappa_2(n, s), \kappa_3(n, s), \kappa_4(n, s)); \\ s &\in [0, S], n = 1, 2, \dots, N \end{aligned} \right\} \quad (7)$$

in which κ_1 , κ_2 , κ_3 and κ_4 represent irregularity types of vertical profile, alignment, cross level and gauge, respectively; s denotes abscissa of the track, S denotes the length of a track irregularity sample; n denotes track irregularity sample number, N denotes the total number of

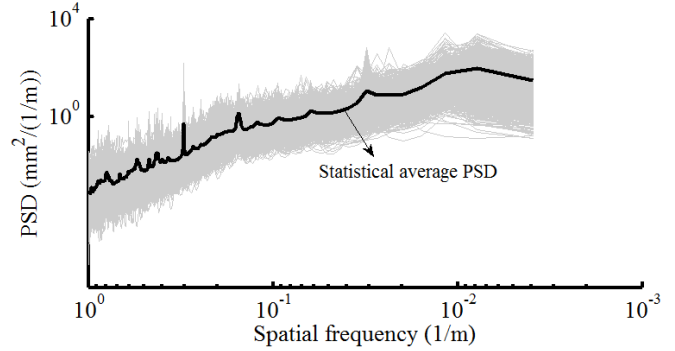


Fig. 3 PSD group of track vertical profile irregularity

irregularity samples.

It is shown that the track irregularity vector contained in Eq. (5) is measured as time domain signals, which can be equivalently transformed as sample set in frequency aspect, namely

$$\left\{ \begin{aligned} \tilde{\Theta}(n, \omega) &= (\tilde{\kappa}_1(n, \omega), \tilde{\kappa}_2(n, \omega), \tilde{\kappa}_3(n, \omega), \tilde{\kappa}_4(n, \omega)); \\ \omega &\in [\omega_l, \omega_u] \end{aligned} \right\} \quad (8)$$

in which $\tilde{\kappa}(\cdot)$ is the PSD results of $\kappa(\cdot)$; ω is the frequency, ω_l and ω_u represent lower- and upper-frequency; $\tilde{\Theta}$ is the random vector of track irregularity sets at frequency domain.

As plotted in Fig. 3, the measured track vertical profile irregularity, i.e., $\kappa_1(n, s)$, from a Chinese high-speed line at track portions of almost 600 kilometers is statistically represented by a group of track irregularity PSD vector, namely $\tilde{\kappa}_1(n, \omega)$, in which each PSD line is obtained from a track irregularity sample with length of 1 km. From Fig. 3, one can observe that the PSDs of track irregularity at different frequencies may differ with 4 orders of magnitude, through investigations, it is feasible to suppose that the PSD lines in Fig. 3 are all assigned with certain probabilities. Conventionally, in most literatures (Zhai *et al.* 2009, Zhang *et al.* 2010, Yu *et al.* 2016), only the statistical average PSD is loaded as the excitation. But undoubtedly, this kind of single-spectrum-excitation (SSE) mode can not reveal all dynamic behaviours of vehicle-track system, especially extreme response and statistical probability distribution, because of the incomplete consideration of track geometries with higher/lower energy levels. In this paper, it is attempted to generate some representative track irregularity samples from the PSD group using a probabilistic method developed by Xu and Zhai (2017).

3.2 Modelling process

Set $\tilde{\kappa}_1(n, \omega)$ as an example, there exists N PSD values for $\tilde{\kappa}_1(\cdot, \omega_i)$ in which ω_i is the i th frequency point. Obviously, the values in $\tilde{\kappa}_1(\cdot, \omega_i)$ obey certain probability density function (PDF) or cumulative density function (CDF). Based on the incremental feature of CDF, one can

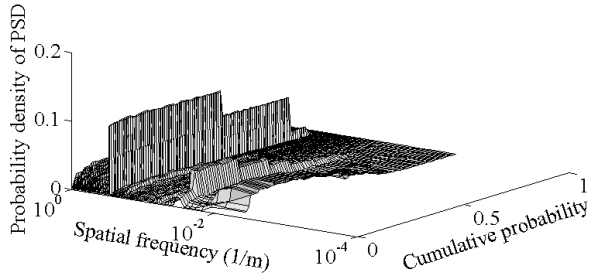


Fig. 4 Joint PDF of track irregularity PSD against spatial frequency and cumulative probability

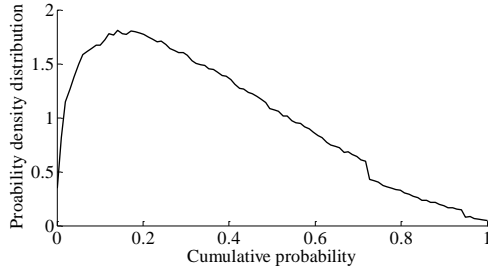


Fig. 5 Probability density distribution of track irregularity PSD against different cumulative probabilities (set track vertical profile irregularity as example)

further describe $\tilde{\kappa}_1(\cdot, \omega_i)$ as the function of wavelength and cumulative probability, namely

$$N(\tau, \omega) = \{\tilde{\kappa}_1(\tau_{\tilde{m}}, \omega_i) \mid \tau_{\tilde{m}} = [\tau_l, \tau_u]; \omega_i = [\omega_l, \omega_u]\} \quad (9)$$

where $N(\tau, \omega)$ denotes track irregularity cumulative probability PS; τ_i represents cumulative probability; τ_u and τ_l are the upper- and lower- boundary cumulative probability, respectively.

Fig. 4 plots a case illustrating the distribution of $N(\tau, \omega)$, from which one can observe that track irregularity at characteristic frequency will possess higher probability density than that of other frequencies. Besides, for PSDs over certain frequency point, their probability density will experience a tendency towards increasing firstly, and then decreasing.

Through the deduction conducted by Xu and Zhai (2017), one is informed that probability of each track irregularity PSD at arbitrary cumulative probability can be calculated by

$$\Gamma(\tilde{\kappa}_1(\tau_{\tilde{m}}, \omega)) = \int_{\tau_{\tilde{m}+1}}^{\tau_{\tilde{m}}} \cdot \int_{\omega_l}^{\omega_u} \Gamma(N(\tau_{\tilde{m}}, \omega)) d\omega \quad (10)$$

Based on Eq. (10), the PDF of track irregularity PSD specified by cumulative probability can be precisely obtained, as shown in Fig. 5.

The result illustrated in Fig. 5 plays a key role in selecting representative and realistic time-domain track irregularities. In addition, it is regarded that all types of track irregularities are mutually independent sets. The methods for selecting representative samples in the random-variate space have been well investigated, e.g., numerical theoretical method (Li and Chen 2007).

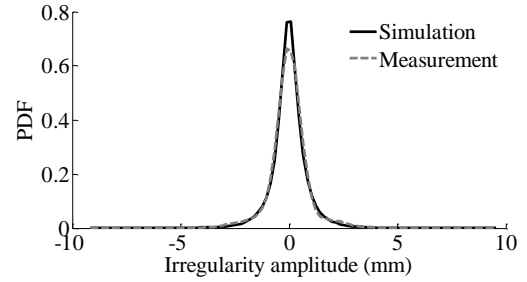


Fig. 6 Comparisons between simulation and measurement for track vertical profile irregularity on PDF

Fig. 6 shows the comparison of probability density distribution of track vertical profile irregularity between simulation and measurement, which serves to illustrate the reliability of the proposed procedures.

4. Rail fastener failure

In the present work, only the failure of rail fasteners is taken into consideration, which will directly lead to the abrupt change of the vertical/lateral stiffness and damping of the track supports, and be viewed as a dangerous factor to the traffic danger, uncomfortableness, and cracks propagation, etc., in a great extent.

The degree of failure of rail fasteners can be characterized by damage coefficient c , namely

$$\begin{aligned} K'_{pv} &= (1 - c_{k,v})K_{pv}; & K'_{ph} &= (1 - c_{k,h})K_{ph}; \\ C'_{pv} &= (1 - c_{c,v})C_{pv}; & C'_{ph} &= (1 - c_{c,h})C_{ph}. \end{aligned} \quad (11)$$

in which $c_{k,v}$, $c_{k,h}$, $c_{c,v}$ and $c_{c,h}$ represent the failure degree of vertical stiffness, lateral stiffness, vertical damping and lateral damping of rail fastener, respectively, and $[c_{k,v}, c_{k,h}, c_{c,v}, c_{c,h}] \in [0, 1]$. The larger of the damage coefficient indicates more serious of the failure.

5. Numerical studies

To compile the mathematical models of railway dynamic systems in which the failure of rail fastener and track random geometries is jointly considered, it is assumed that the vehicle moves at a speed of 350 km per hour on the slab-track guiding system. The parameters for the vehicle and track sub-models are listed in the monograph (Zhai 2015). The track irregularities used in the numerical simulation are simulated from the measured data of a high-speed line.

Through investigations (Zhai 2015), the boundary effect of the tracks on vehicle-track vibrations can be neglected once the track length respectively intercepted from the front and the rear of the vehicle is over 30 meters. In this calculation, the length of the track is chosen as 200 meters.

5.1 Computational conditions

In the numerical studies, it is assumed the rail fasteners

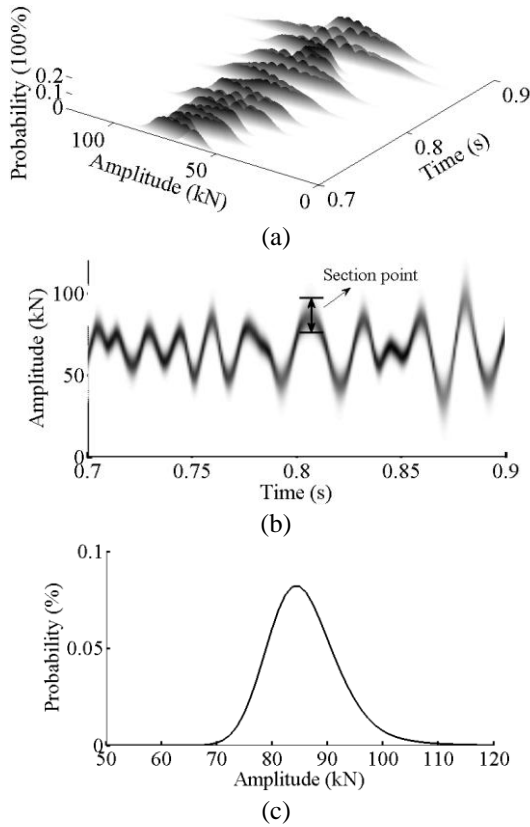


Fig. 7 Probability evolution of W/R VFs against time under condition d: (a) 3-D view; (b) top view; (c) Probability distribution against amplitudes for section point shown in (b)

are in complete failure status, namely $[c_{k,v}, c_{k,h}, c_{c,v}, c_{k,h}] = 1$ at specific track sections. Meanwhile, the normal rail fastener condition $[c_{k,v}, c_{k,h}, c_{c,v}, c_{k,h}] = 0$ is used as a comparative object. Besides, it is regarded that one to four rail fasteners fail for all the above working conditions at different track segments.

5.2 Results and discussions

The complete dynamic responses of the railway vehicle and the track can be obtained by the following steps:

- 1) Accessing N samples of track random irregularities with full scales on amplitudes, wavelengths and probabilities through methods presented in Section 3,
- 2) Dynamic calculations using the vehicle-track coupled model developed in Section 2 with N track irregularity samples included as the exciting sources of railway systems.
- 3) A newly developed probability density evolution method (PDEM) (Li and Chen 2008) will be applied to obtain the PDF of the dynamic results against time denoted by $p_X(x,t)$, in which x is the amplitude of the dynamic response, t represents integration time.

The ranges of response amplitudes and the corresponded probability density evolutions against time can't be revealed in most of the literature, though the dynamic behaviours of indices at time domain can be obtained accompanied by the acquisition of the general features of amplitudes and

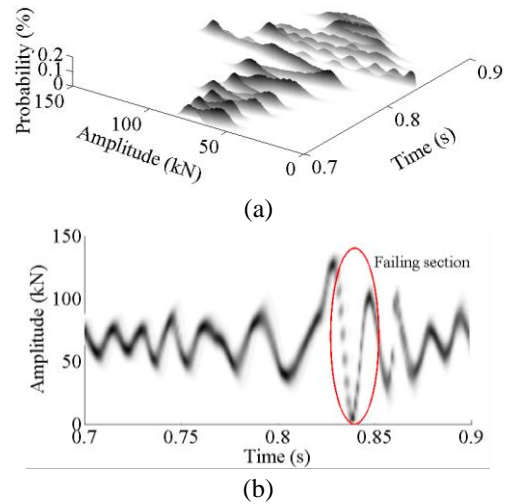


Fig. 8 Probability evolution of W/R VFs against time with four rail fasteners failure: (a) 3-D view; (b) top view

frequencies. However, to railway engineers, the full view of dynamic responses of the railway systems at various working conditions, including both good and worse, and their probabilities of occurrence may be one of the most important concerns. As an illustration, Figs. 7 and 8 show representative results of wheel/rail vertical force (W/R VF) available for comparison between conditions of normal track supports and failure of rail fasteners. Seen from Fig. 7 (a) and (b) that W/R VFs at arbitrary track sections vary in a large range due to the consideration of the ergodic properties of track irregularities, which means that one can be informed all of the responses of the railway systems on effects of random track irregularities by using the strategies presented in this paper. It is illustrated from Fig. 7(c) that the minimum-maximum W/R VF at one track sectional point may differ with 40 kN by accounting for the variations of track random irregularities. When the rail fastener failures happen, the amplitudes, vibration modes, and frequencies will be wholly changed to adapt to this failure.

Normally, when the track support failures encounter with the effects of track random irregularities, the researches on identification of failure and mechanical laws will be in trouble due to the fact that the dynamic behaviours of railway systems caused by support failures will be greatly affected or even covered by the track random irregularities. Therefore, Xiao *et al.* (2007), Mazilu (2010) directly ignored the influence of rail surface irregularities in the dynamic calculations for obtaining more intuitionistic results. However, track random irregularities exist objectively with great influences on railway vehicle-track interactions. Therefore, in this research, it is aimed to clarify the joint influence of track random irregularities and rail fastener failures on dynamic behaviours of railway systems.

At the next two sub-sections, we will expose the dynamic results from two aspects, namely wheel/rail interaction and vibrations of the tracks, and mainly adopt two indicators, namely mathematical expectation $E_X(t)$ and standard deviation $\delta_X(t)$ to characterize the variance of

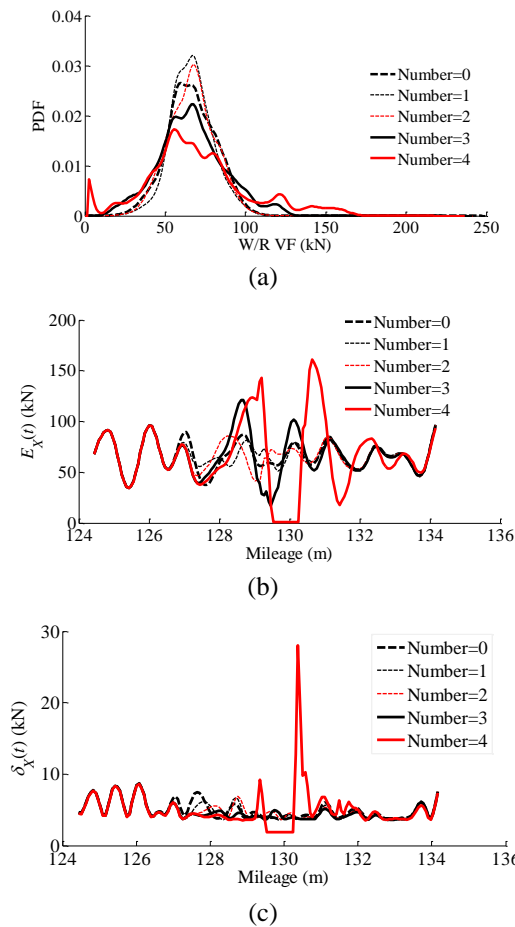


Fig. 9 Dynamic results of W/R VF at mileage segment M2: (a) PDF (b) $E_X(t)$ (c) $\delta_X(t)$

dynamic response caused by track random irregularities and the failure of rail fasteners.

5.2.1 On the wheel/rail interaction

Fig. 9 plots the dynamic results, i.e., the average PDF, mathematical expectation $E_X(t)$ and standard deviation $\delta_X(t)$ of W/R VF, of specific track section with rail fastener failures of number=0, 1, 2, 3 and 4 included. One can observe from Fig. 9(a) that the PDFs of W/R VF will be changed along with the failures of rail fasteners, especially when the failing number reaches 4, the variation scope of W/R VF will almost reach the limits, namely W/R VF=0 that indicates wheel off the rail, and W/R VF=170 which is the limit of maximum vertical force. As for random responses, Generally, it is assumed the maximum-minimum values of responses will be in the range of $[E_X(t)-3\delta_X(t), E_X(t)+3\delta_X(t)]$ with probability of 99.74% regarding to Gaussian distribution, so the $E_X(t)$ and $\delta_X(t)$ are two of the most important indicators in characterizing the variation ranges of random signals. As shown from Fig. 9, the dynamic variation at the track failure portion is rather obvious when failing number is 3 or 4, however, the influence of rail fastener failure is unobvious if the failing number is relatively lesser, e.g., number=1 or 2.

From Fig. 9, the effects of rail fastener failure on W/R VF is rather clear that the rail support failures will

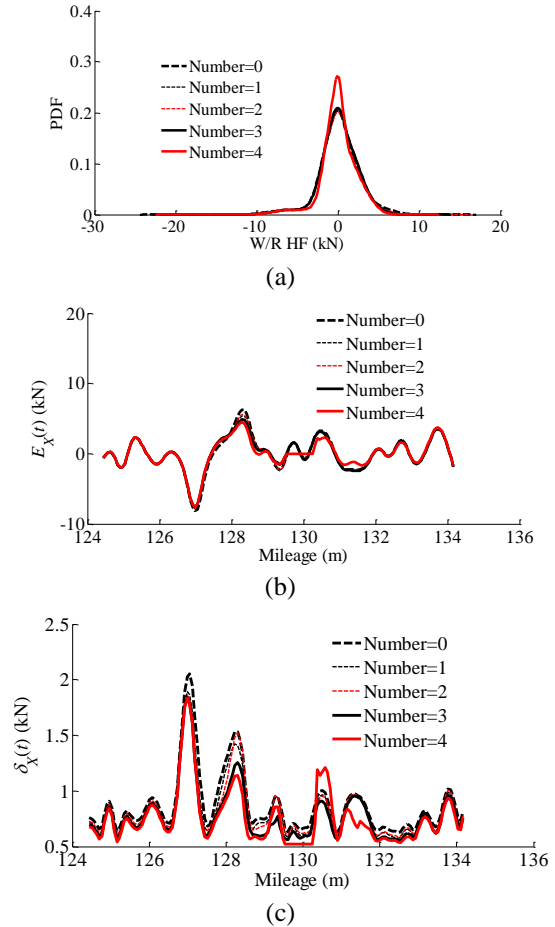


Fig. 10 Dynamic results of W/R HF at mileage segment M2: (a) PDF (b) $E_X(t)$ (c) $\delta_X(t)$

obviously intensify the wheel/rail vertical interactions. However, when considering the wheel/rail lateral force (W/R LF), the participation of track random irregularity will highlight its importance on guiding the wheel/rail lateral interaction, though the failure of rail fastener system has impacts on it as well. One can observe from Fig. 10 the maximum values of mathematical expectation and standard deviation (the square of variance) occur at mileage 128.4 m at normal rail support condition, which indicates that track random irregularities play decisive role in determining the dynamic trajectories of wheel/rail lateral interaction.

Besides, it is predictable from Fig. 10 that the wheel/rail lateral interaction is relatively more complicate than vertical interaction for being hard to capture the weak variances in response amplitudes, however, the frequency features of W/R LF has been significantly altered by the rail fastener failures. It may be another important matter needed to be probed into. Illustrated in Fig. 11 is the frequency spectra of $E_X(t)$ of W/R VF and W/R LF, respectively. To W/R VF, when the failing of rail fasteners is in wide range, it is easy to form impulse signals on W/R VF. Thus, the spectral values of Number=4 are obviously higher than other conditions almost at the whole frequency range. Being very different from the vertical vibration, spectral values obtained at the status of rail support failure, i.e., Number=1, 2, 3 and 4, may be lower than normal rail support condition

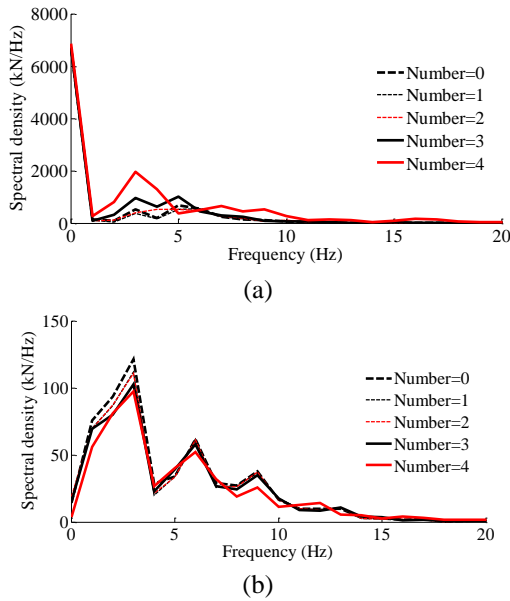


Fig. 11 Frequency spectra of $E_X(t)$: (a) W/R VF; (b) W/R LF

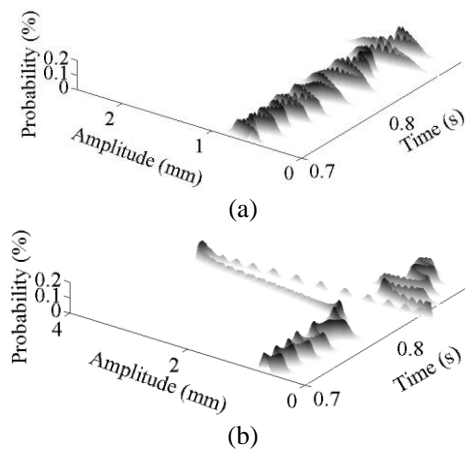


Fig. 12 PDF surface of vertical displacement of the rail against time: (a) Number=0; (b) Number=4

(Number=0) due to the fact that the reduction of rail lateral stiffness may weaken the wheel/rail LF, this result is in accordance with the conclusion of the monograph (Zhai 2015).

5.2.2 On the tracks

Fig. 12 plots the PDF surface of rail vertical displacement against time for conditions of Number=0 and Number=4, respectively. From Fig. 12, one can observe that the rail displacement has been greatly amplified due to the failure of rail support. The maximum displacement of Number=4 has been raised 3.37 times against that of Number=0 from value of 1.05 mm into 3.54 mm.

Meanwhile, Figs. 13 and 14 plot the time-dependent mathematical expectation $E_X(t)$ and standard deviation $\delta_X(t)$ of rail vertical and lateral acceleration, respectively. It is clear the failure of rail support has great impacts on vertical and lateral vibrations of the rails. To rail vertical accelerations, the effects mainly appear at large rail support

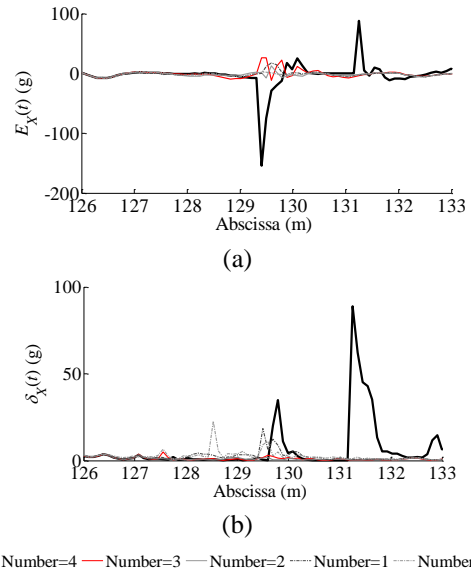


Fig. 13 Statistical indexes of vertical acceleration of the rail: (a) $E_X(t)$; (b) $\delta_X(t)$

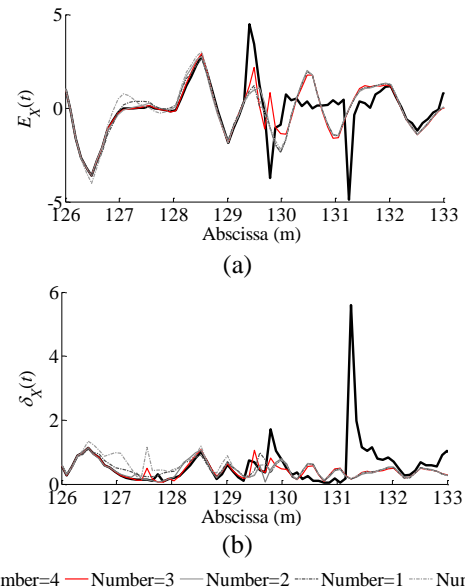


Fig. 14 Statistical indexes of lateral acceleration of the rail: (a) $E_X(t)$; (b) $\delta_X(t)$

failing status, e.g., Number=3 and 4. Especially when the number of rail fastener failure reaches 4, the average responses of rail accelerations will be boosted with dozens of times, as shown in Fig. 13. Similarly, seen from Fig. 14, the influence of rail support failing on lateral vibrations of rails is also significant.

6. Conclusions

It is sometimes a hard work to clarify the track portions where the rail support failure may happen at. Thus it is a necessity to assess the dynamic responses of railway systems when the structural failure occurs. And it is inevitable to take track random irregularities into the

consideration jointly, due to their significant influence on wheel/rail interactions.

Within the framework of this study, it becomes feasible to evaluate the influence of rail support failure on railway system dynamics in a more reliable way by getting closer to the actual wheel/rail working status with rail geometric deformations considered. Employing the simulation method of track random irregularities, we can obtain all of the track irregularities that may emerge on the rail profiles at present or possibly future. Therefore, with the assistance of the vehicle-track coupled model, it is convenient to quantitatively evaluate the dynamic behaviours of the railway vehicles and the tracks through jointly accounting for the structural failures and track random irregularities.

Through numerical studies of this paper, several conclusions can be drawn:

- 1) It is clarified that the failure of rail fastener has significant impacts on the railway vehicle-track vibrations, especially on vertical vibrations of the wheel/rail systems and the tracks.
- 2) The wheel/rail lateral force may be mitigated because of the reductions of the rail lateral stiffness, but simultaneously, the rail lateral deformation will be increased contrarily. So it is rather important to choose the rail lateral stiffness reasonably.
- 3) With the methods developed in this study, it is approachable to bound the response regions of dynamic indices under the condition of structural failure and random track irregularities with two statistical indicators, i.e., mathematical expectation and standard deviation.
- 4) It is confident to demonstrate that the running safety of the railway vehicle can be guaranteed in current track geometric status of this railway, if the number of continuous failure of rail fasteners is limited within two. Besides, the probability of over limits is relatively very small for wheel/rail forces even if the failing number is four.

Acknowledgements

This work was supported by [the National Basic Research Program of China ("973" Program)] under Grant [number 2013CB036206, 2013CB036205]; [The National Natural Science Fund] under Grant [number 51478482; 51678507]; the Program of Introducing Talents of Discipline to Universities (111 Project) [number B1604].

References

Andersson, R., Torstensson, P. T., Kabo, E. and Larsson, F. (2015), "An efficient approach to the analysis of rail surface irregularities accounting for dynamic train-track interaction and inelastic deformations", *Veh. Syst. Dyn.*, **53**, 1667-1685.

Carrascal, I.A., Casado, J.A., Diego, S. and Polanco, J.A. (2016), "Dynamic behavior of high-speed rail fastenings in the presence of desert sand", *Constr. Build. Mater.*, **117**, 220-228.

Chen, G. and Zhai, W.M. (2004), "A new wheel/rail spatially dynamic coupling model and its verification", *Veh. Syst. Dyn.*,

41, 301-322.

Chen, J.B., Sun, W.L., Li, J. and Xu, J. (2013), "Stochastic harmonic function representation of stochastic processes", *J. Appl. Mech.*, **80**(1), 011001.

Chen, Z., Shin, M., Andrawes, B. and Edwards, J.R. (2014), "Parametric study on damage and load demand of prestressed concrete cross-tie and fastening systems", *Eng. Fail. Anal.*, **46**, 49-61.

Domingo, L.M., Giner, B.B., Martin, C.Z. and Herraiz, J.I.R. (2014), "Experimental modal analysis of transverse-cracked rails-influences of the cracks on the real track behavior", *Struct. Eng. Mech.*, **52**(5), 1019-1032.

Hussein, M.F. and A. Costa, P. (2016), "The effect of end bearings on the dynamic behaviour of floating-slab tracks with discrete slab units", *Int. J. Rail Tran.*, **5**(1), 38-46.

Ilias, H. (1999), "The influence of railpad stiffness on wheelset/track interaction and corrugation growth", *J. Sound Vib.*, **227**(5), 935-948.

Li, J. and Chen, H.B. (2008), "The principle of preservation of probability and the generalized density evolution Eq.", *Struct. Saf.*, **30**, 65-77.

Li, J. and Chen, J.B. (2007), "The numerical theoretical method in response analysis of nonlinear stochastic structures", *Comput. Mech.*, **39**(6), 693-708.

Li, Z., Zhao, X. and Dollevoet, R. (2016), "An approach to determine a critical size for rolling contact fatigue initiating from rail surface defects", *Int. J. Rail Tran.*, **5**(1), 16-37.

Maes, J., Sol, H. and Guillaume, P. (2006), "Measurements of the dynamic railpad properties", *J. Sound Vib.*, **293**, 557-565.

Mazilu, T. (2010), "Prediction of the interaction between a simple moving vehicle and an infinite periodically supported rail-Green's functions approach", *Veh. Syst. Dyn.*, **48**(9), 1021-1042.

Oregui, M., Li, Z. and Dollevoet, R. (2015), "An investigation into the modelling of railway fastening", *Int. J. Mech. Sci.*, **92**, 1-11.

Pålsson, B.A. and Nielsen, J.C. (2015), "Dynamic vehicle-track interaction in switches and crossings and the influence of rail pad stiffness-field measurements and validation of a simulation model", *Veh. Syst. Dyn.*, **53**(6), 734-755.

Shen, Z.Y., Hedrick, J.K. and Elkins, J.A. (1983), "A comparison of alternative creep force models for rail vehicle dynamic analysis", *Proceedings of 8th IAVSD Symposium*, MIT, Cambridge, June.

Smutny, J. (2004), "Measurement and analysis of dynamic and acoustic parameters of rail fastening", *NDT & E Int.*, **37**, 119-129.

Thompson, D.J. and Verheij, J.W. (1997), "The dynamic behaviour of rail fasteners at high frequencies", *Appl. Acoust.*, **52**(1), 1-17.

Xiao, X., Jin, X. and Wen, Z. (2007), "Effect of disabled fastening systems and ballast on vehicle derailment", *J. Vib. Acoust.*, **129**, 217-229.

Xiao, X., Jin, X., Deng, Y. and Zhou, Z. (2008), "Effect of curved track support failure on vehicle derailment", *Veh. Syst. Dyn.*, **46**(11), 1029-1059.

Xu, L. and Zhai, W. (2017), "A new model for temporal-spatial stochastic analysis of vehicle-track coupled systems", *Veh. Syst. Dyn.*, **55**(3), 427-448.

Xu, L. and Zhai, W. (2017), "A novel model for determining the amplitude-wavelength limits of track irregularities accompanied by a reliability assessment in railway vehicle-track dynamics", *Mech. Syst. Signal Pr.*, **86**, 260-277.

Xu, L., Zhai, W. and Gao, J. (2017), "Extended applications of track irregularity probabilistic model and vehicle-slab track coupled model on dynamics of railway systems", *Veh. Syst. Dyn.*, 1-21.

Yu, Z.W., Mao, J.F., Guo, F.Q. and Guo, W. (2016), "Non-stationary random vibration analysis of a 3D train-bridge system using the probability density evolution method", *J. Sound Vib.*,

366, 173-189.

- Zeng, Z.P., He, X.F., Zhao, Y.G., Yu, Z.W., Chen, L.K., Xu, W.T. and Lou, P. (2015), "Random vibration analysis of train-slab track-bridge coupled system under earthquakes", *Struct. Eng. Mech.*, **54**(5), 1017-1044.
- Zhai, W. (2015), *Vehicle-track Coupled Dynamics*, the 4th Edition, Science Press, Beijing.
- Zhai, W., Wang, K. and Cai, C. (2009), "Fundamentals of vehicle-track coupled dynamics", *Veh. Syst. Dyn.*, **47**, 1349-1376.
- Zhang, Z.C., Lin, J.H., Zhang, Y.H., Zhao, Y., Jowson, W.P. and Williams, F.W. (2010), "Non-stationary random vibration analysis for train-bridge systems subjected to horizontal earthquakes", *Eng. Struct.*, **32**, 3571-3582.
- Zhu, S., Cai, C. and Spanos, P.D. (2015), "A nonlinear and fractional derivative viscoelastic model for rail pads in the dynamic analysis of coupled vehicle-slab track systems", *J. Sound Vib.*, **335**, 304-320.

CC